

Bending and Free Vibration Analysis of Functionally Graded Sandwich Plates with porosity using Higher-Order Shear Deformation Theory

Lan Hoang Ton-That*

Faculty of Civil Engineering, University of Architecture Ho Chi Minh City, Vietnam

*email: tonthathoanglan.247@gmail.com

ABSTRACT

In this paper, for the first time, the bending and free vibration analysis of porous functionally graded sandwich (PFGS) plates is investigated using a higher-order shear deformation theory (HSDT) C0 type and finite element model. This construction consists of a single homogenous ceramic core and two distinct functionally graded skins. The mechanical results related to bending and free vibration behaviours of it are searched using the Matlab software. The other plates with different materials or arbitrary forms can use this code as well in the future. To verify the procedure's potential of use, the study's findings are contrasted with those of previous studies in the literature. Additionally, the effects of a number of parameters on the bending and vibration of PFGS plates are provided, including the porosity factor, volume fraction index, and geometric ratio. These results show that the distribution of porosity plays a significant role in the mechanical properties of PFGS plates.

Keywords: Sandwich plate; functionally graded material; porosity; finite element analysis

1.0 INTRODUCTION

These days, many modern fields have specific criteria that traditional materials' mechanical qualities do not meet. A team of Japanese scientists developed very advantageous functionally graded materials in 1984. Following that, these smart materials have been used much more frequently. This material offers a continuous variation of properties from the top surface to the bottom surface and it is composed of a metal and ceramic blend. There are now more applications in the fields of nuclear power plants, defense engineering, aerospace and submarine engineering, etc. In general, analytical solutions [1-4] have always had limitations. Because of the shear locking free, the third-order shear deformation plate theories are precise and efficient substitutes. A straightforward third-order shear deformation plate theory was recently provided by Shi [5] to examine the static behaviours of beam/plate constructions. It has been suggested that the outcomes produced by this theory are more applicable than others. On the other hand, structural analyses typically employ numerical approaches. A unified and integrated strategy for the enhancement of the Felippa Bergan triangular element from thin to thick plates was provided in [6]. The suggested element produced satisfactory results in the common benchmark issues for isotropic plates and sandwich plates with functionally graded materials, free of locking, and an appropriate rank. A higher-order layerwise finite element formulation for static and dynamic assessments of sandwich plates made of functionally graded materials was described in [7]. To maintain continuity of displacement at the layer interface, a higher-order displacement field was postulated for the core and a first-order displacement field for the top and bottom face sheets. In this work, an eight-noded isoparametric element with thirteen degrees of freedom per node has been investigated for two configurations of sandwich plates with functionally graded materials utilizing a C0-based finite element formulation. Additionally, the research [8-15] provided multiple applications of various theories to the study of functionally graded sandwich structure bending, free vibration, and buckling. Conversely, the authors of [16-18] investigated how material uncertainties affect the bending and vibration characteristics of sandwich plates with functional grades. They also concentrated on the study of stress and deformation, or the extension of the unified formulation of Carrera in polar coordinates of such studies. The works [19-22] also introduced a new model for the fully coupled thermo-mechanical static analysis of multilayered plates with embedded functionally graded material layers, either skins or core layers, under mechanical or thermal loads. This new model could be used with the Navier approach, the Fourier series, the Mori-Tanaka estimates, or a new inverse trigonometric shear deformation theory. Furthermore, prior research [23-26] has demonstrated the benefits of the four-node quadrilateral element in the analysis of plate and shell structures. These could be viewed as particular examples of how analysis might be extended to include constructions that use smart materials. Last but not least, the phenomena of shear locking, membrane locking, or hourglass in finite element analysis of plate

and shell structures have also been introduced in depth in some previous investigations [27–30], like opening up the right path in structural calculation.

Back to this study, the finite element procedure for PFGS plates based on Shi's theory with C^0 form is the main task. More specifically, this theory was proposed in [5], accompanied by analytical solutions obtained and verified for accuracy when compared with 3D elastic solutions. However, the author applied Shi theory combined with the finite element algorithm related to C^0 form to produce numerical solutions, as presented in [11], for the structural analysis of plates made of functionally graded materials. The novelty here is the attempt to extend Matlab code for the analysis to PFGS plates, by considering the influence of porosity. The next parts of this paper are given as follows. The concept of material, including two cases of porosity, the change of material properties, and the procedure for static bending and frequency analyses, are presented in Part 2. The numerical results are shown in Part 3, and some comments are presented in the last part.

2.0 FORMULATION

Firstly, Figure 1 shows a plot of a sandwich plate that has been functionally graded. The z -axis is perpendicular to the xy -plane, which is the plate's mid-plane. Additionally, its structure consists of one homogenous ceramic core and two distinct functionally graded skins.

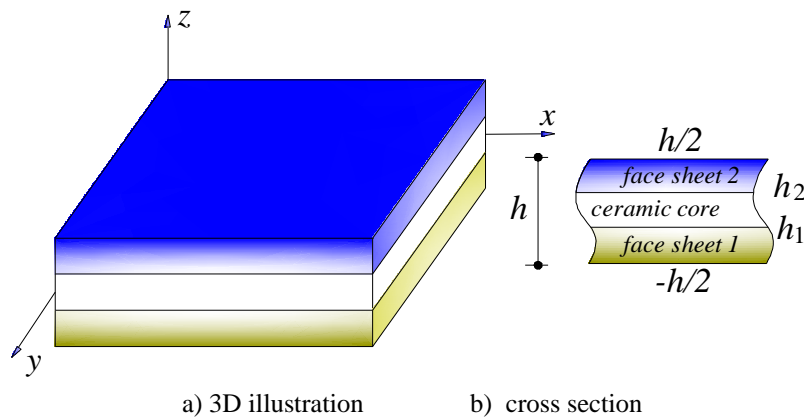


Figure 1. The functionally graded sandwich plate with two face sheets and one ceramic core

The study examines two situations of porous distribution: i) type I with even porous face sheets; and ii) type II with linear-uneven porous core, based on the appearance of porosity related to the porosity factor e in this structure. For two varieties, the material properties $M(z)$ are provided:

Type I

$$\left\{ \begin{array}{l} M(z) = M_b + (M_c - M_b) \left(\frac{z + h/2}{h_1 + h/2} \right)^n - (M_c + M_b) \frac{e}{2} \quad -h/2 \leq z \leq h_1 \\ M(z) = M_c \quad h_1 < z < h_2 \\ M(z) = M_t + (M_c - M_t) \left(\frac{z - h/2}{h_2 - h/2} \right)^n - (M_c + M_b) \frac{e}{2} \quad h_2 \leq z \leq h/2 \end{array} \right. \quad (1)$$

Type II

$$\left\{ \begin{array}{l} M(z) = M_b + (M_c - M_b) \left(\frac{z + h/2}{h_1 + h/2} \right)^n \quad -h/2 \leq z \leq h_1 \\ M(z) = M_c - eM_c \left(1 - \frac{|2z - h_1 - h_2|}{h_2 - h_1} \right) \quad h_1 < z < h_2 \\ M(z) = M_t + (M_c - M_t) \left(\frac{z - h/2}{h_2 - h/2} \right)^n \quad h_2 \leq z \leq h/2 \end{array} \right. \quad (2)$$

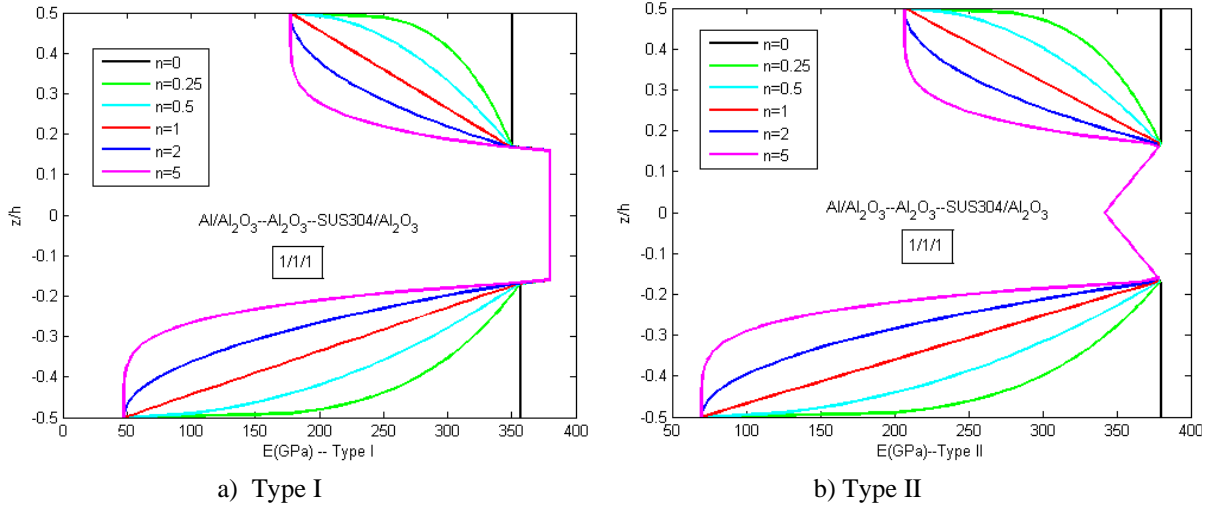


Figure 2. The modification of E with $e = 0.1$ for Type I & II and ratio of the thicknesses [1/1/1]

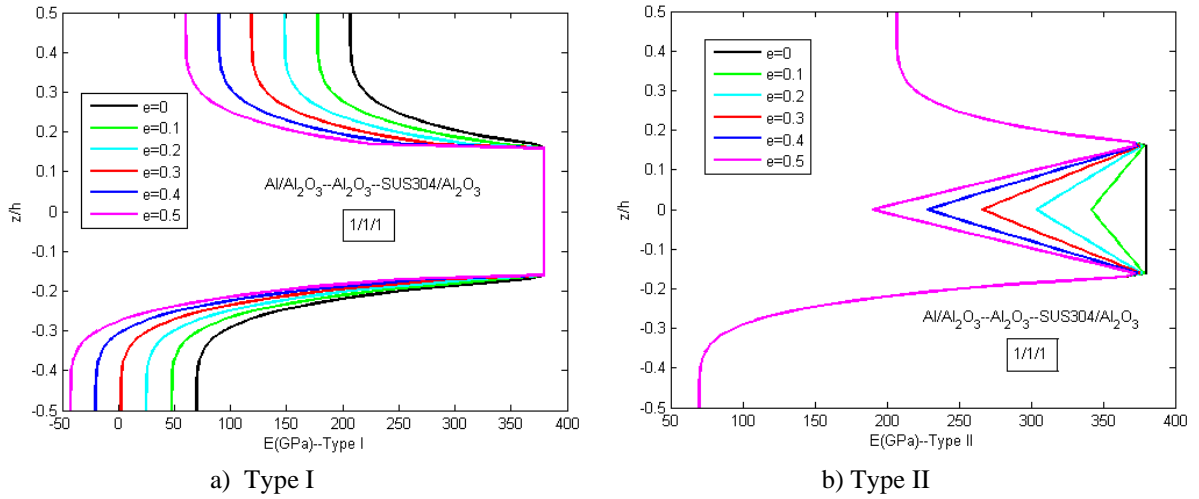


Figure 3. The modification of E with $n = 5$ for Type I & II and ratio of the thicknesses [1/1/1]

Three digits, such as " $t_1 / t_2 / t_3$," indicate the ratio of the thicknesses of the top, bottom, and core layers. $h.t_1 / (t_1 + t_2 + t_3)$ represents the bottom skin, $h.t_2 / (t_1 + t_2 + t_3)$ represents the core layer, and $h.t_3 / (t_1 + t_2 + t_3)$ represents the top skin. Figures 2 and 3 show the variation of E by changing the material parameters of the sandwich plate $Al/Al_2O_3 + Al_2O_3 + SUS304/Al_2O_3$ for both Types I and II.

With two additional variables added, the displacement field can be expressed in terms of C^0 -HSDT based on Shi's theory [5] and a slight modification [11]. To compute a low-order quadrilateral element with four nodes, all that is needed is the first derivative of transverse displacement. The unknown variables are currently shown as follows:

$$u(x, y, z) = u_0(x, y) + \left(\frac{1}{4}z - \frac{5}{3h^2}z^3 \right) \phi_x^b + \frac{5}{4} \left(z - \frac{4}{3h^2}z^3 \right) \phi_x^s(x, y) \quad (3)$$

$$v(x, y, z) = v_0(x, y) + \left(\frac{1}{4}z - \frac{5}{3h^2}z^3 \right) \phi_y^b + \frac{5}{4} \left(z - \frac{4}{3h^2}z^3 \right) \phi_y^s(x, y) \quad (4)$$

$$w(x, y, z) = w_0(x, y) \quad (5)$$

With these seven unknowns, three displacements and four rotations due to the bending and shear effects, the displacement-strain relations can be written in matrix form.

$$\boldsymbol{\varepsilon} = \begin{Bmatrix} u_{0,x} \\ v_{0,y} \\ u_{0,y} + v_{0,x} \end{Bmatrix} + z \frac{1}{4} \begin{Bmatrix} (5\phi_{x,x}^s + \phi_{x,x}^b) \\ (5\phi_{y,y}^s + \phi_{y,y}^b) \\ (5\phi_{x,y}^s + 5\phi_{y,x}^s + \phi_{x,y}^b + \phi_{y,x}^b) \end{Bmatrix} + z^3 \frac{-5}{3h^2} \begin{Bmatrix} \phi_{x,x}^s + \phi_{x,x}^b \\ \phi_{y,y}^s + \phi_{y,y}^b \\ \phi_{x,y}^s + \phi_{x,y}^b + \phi_{y,x}^s + \phi_{y,x}^b \end{Bmatrix} \quad (6)$$

$$\boldsymbol{\gamma} = \begin{Bmatrix} \frac{5}{4}\phi_y^s + \frac{1}{4}\phi_y^b + w_{,y} \\ \frac{5}{4}\phi_x^s + \frac{1}{4}\phi_x^b + w_{,x} \end{Bmatrix} + z^2 \frac{-5}{h^2} \begin{Bmatrix} \phi_y^s + \phi_y^b \\ \phi_x^s + \phi_x^b \end{Bmatrix} \quad (7)$$

The constitutive equation is expressed as

$$\boldsymbol{\sigma} = \mathbf{D}_m(z)\boldsymbol{\varepsilon} \quad (8)$$

$$\boldsymbol{\tau} = \mathbf{D}_s(z)\boldsymbol{\gamma} \quad (9)$$

in which

$$\boldsymbol{\sigma} = [\sigma_x \quad \sigma_y \quad \sigma_{xy}]^T; \quad \boldsymbol{\tau} = [\tau_{yz} \quad \tau_{xz}]^T \quad (10)$$

$$\mathbf{D}_m(z) = \frac{E(z)}{1-\nu(z)^2} \begin{bmatrix} 1 & \nu(z) & 0 \\ \nu(z) & 1 & 0 \\ 0 & 0 & (1-\nu(z))/2 \end{bmatrix}; \quad \mathbf{D}_s(z) = \frac{E(z)}{2(1+\nu(z))} \begin{bmatrix} 1 & 0 \\ 0 & 1 \end{bmatrix} \quad (11)$$

The generalized displacements can hence be approximated as

$$\mathbf{u}_0 = \mathbf{N}\mathbf{q}_e \quad (12)$$

with

$$\mathbf{u}_0 = [u_0 \quad v_0 \quad w \quad \phi_x^s \quad \phi_y^s \quad \phi_x^b \quad \phi_y^b]^T; \quad \mathbf{N} = [N_1 \quad N_2 \quad N_3 \quad N_4]; \quad \mathbf{q}_e = [\mathbf{q}_{1e} \quad \mathbf{q}_{2e} \quad \mathbf{q}_{3e} \quad \mathbf{q}_{4e}]^T \quad (13)$$

\mathbf{q}_e and \mathbf{N} are the unknown displacement vector and the shape function vector. The strain can be rewritten as

$$(\mathbf{B}_1 + \mathbf{B}_2 + \mathbf{B}_3)\mathbf{q}_e = \boldsymbol{\varepsilon} \quad (14)$$

$$(\mathbf{B}_4 + \mathbf{B}_5)\mathbf{q}_e = \boldsymbol{\gamma} \quad (15)$$

in which

$$\mathbf{B}_1 = \sum_{i=1}^4 \begin{bmatrix} \mathbf{N}_{i,x} & 0 & 0 & 0 & 0 & 0 & 0 \\ 0 & \mathbf{N}_{i,y} & 0 & 0 & 0 & 0 & 0 \\ \mathbf{N}_{i,y} & \mathbf{N}_{i,x} & 0 & 0 & 0 & 0 & 0 \end{bmatrix}; \quad \mathbf{B}_2 = \frac{1}{4} \sum_{i=1}^4 \begin{bmatrix} 0 & 0 & 0 & 5\mathbf{N}_{i,x} & 0 & \mathbf{N}_{i,x} & 0 \\ 0 & 0 & 0 & 0 & 5\mathbf{N}_{i,y} & 0 & \mathbf{N}_{i,y} \\ 0 & 0 & 0 & 5\mathbf{N}_{i,y} & 5\mathbf{N}_{i,x} & \mathbf{N}_{i,y} & \mathbf{N}_{i,x} \end{bmatrix} \quad (16)$$

$$\mathbf{B}_3 = -\frac{5}{3h^2} \sum_{i=1}^4 \begin{bmatrix} 0 & 0 & 0 & \mathbf{N}_{i,x} & 0 & \mathbf{N}_{i,x} & 0 \\ 0 & 0 & 0 & 0 & \mathbf{N}_{i,y} & 0 & \mathbf{N}_{i,y} \\ 0 & 0 & 0 & \mathbf{N}_{i,y} & \mathbf{N}_{i,x} & \mathbf{N}_{i,y} & \mathbf{N}_{i,x} \end{bmatrix} \quad (17)$$

$$\mathbf{B}_4 = \sum_{i=1}^4 \begin{bmatrix} 0 & 0 & \mathbf{N}_{i,y} & 0 & \frac{5}{4} & 0 & \frac{1}{4} \\ 0 & 0 & \mathbf{N}_{i,x} & \frac{5}{4} & 0 & \frac{1}{4} & 0 \end{bmatrix}; \quad \mathbf{B}_5 = -\frac{5}{h^2} \sum_{i=1}^4 \begin{bmatrix} 0 & 0 & 0 & 0 & 1 & 0 & 1 \\ 0 & 0 & 0 & 1 & 0 & 1 & 0 \end{bmatrix} \quad (18)$$

The components of forces and moments can be introduced as

$$\begin{aligned}\bar{\mathbf{N}} &= \bar{\mathbf{A}}\boldsymbol{\varepsilon}^{(0)} + \bar{\mathbf{B}}\boldsymbol{\varepsilon}^{(1)} + \bar{\mathbf{E}}\boldsymbol{\varepsilon}^{(3)}; & \bar{\mathbf{M}} &= \bar{\mathbf{B}}\boldsymbol{\varepsilon}^{(0)} + \bar{\mathbf{D}}\boldsymbol{\varepsilon}^{(1)} + \bar{\mathbf{F}}\boldsymbol{\varepsilon}^{(3)}; \\ \bar{\mathbf{P}} &= \bar{\mathbf{E}}\boldsymbol{\varepsilon}^{(0)} + \bar{\mathbf{F}}\boldsymbol{\varepsilon}^{(1)} + \bar{\mathbf{H}}\boldsymbol{\varepsilon}^{(3)} \\ \bar{\mathbf{Q}} &= \hat{\mathbf{A}}\boldsymbol{\gamma}^{(0)} + \hat{\mathbf{B}}\boldsymbol{\gamma}^{(2)}; & \bar{\mathbf{R}} &= \hat{\mathbf{B}}\boldsymbol{\gamma}^{(0)} + \hat{\mathbf{D}}\boldsymbol{\gamma}^{(2)}\end{aligned}\quad (19)$$

With

$$\bar{\mathbf{A}} = \int_{-h/2}^{h/2} \mathbf{D}_m(z) dz, \quad \bar{\mathbf{B}} = \int_{-h/2}^{h/2} z \mathbf{D}_m(z) dz, \quad \bar{\mathbf{D}} = \int_{-h/2}^{h/2} z^2 \mathbf{D}_m(z) dz \quad (20)$$

$$\bar{\mathbf{E}} = \int_{-h/2}^{h/2} z^3 \mathbf{D}_m(z) dz, \quad \bar{\mathbf{F}} = \int_{-h/2}^{h/2} z^4 \mathbf{D}_m(z) dz, \quad \bar{\mathbf{H}} = \int_{-h/2}^{h/2} z^6 \mathbf{D}_m(z) dz \quad (21)$$

$$\hat{\mathbf{A}} = \int_{-h/2}^{h/2} \mathbf{D}_s(z) dz, \quad \hat{\mathbf{B}} = \int_{-h/2}^{h/2} z^2 \mathbf{D}_s(z) dz, \quad \hat{\mathbf{D}} = \int_{-h/2}^{h/2} z^4 \mathbf{D}_s(z) dz \quad (22)$$

Given the normal forces, shear force, bending moments, and higher-order moments acting on a plate, the total strain energy may be calculated using

$$U = \frac{1}{2} \int_{V_e} \boldsymbol{\varepsilon}^T \boldsymbol{\sigma} dV - \int_{S_e} \mathbf{u}^T \mathbf{f} dS = \frac{1}{2} \mathbf{q}_e^T \int_{S_e} \Upsilon dS \mathbf{q}_e - \mathbf{q}_e^T \int_{S_e} \mathbf{N}^T \mathbf{f} dS \quad (23)$$

$$U = \frac{1}{2} \mathbf{q}_e^T \mathbf{K}_e \mathbf{q}_e - \mathbf{q}_e^T \mathbf{F}_e = \mathbf{q}_e^T \left(\frac{1}{2} \mathbf{K}_e \mathbf{q}_e - \mathbf{F}_e \right) \quad (24)$$

in which

$$\begin{aligned}\Upsilon &= \mathbf{B}_1^T \bar{\mathbf{A}} \mathbf{B}_1 + \mathbf{B}_1^T \bar{\mathbf{B}} \mathbf{B}_2 + \mathbf{B}_1^T \bar{\mathbf{E}} \mathbf{B}_3 + \mathbf{B}_2^T \bar{\mathbf{B}} \mathbf{B}_1 + \mathbf{B}_2^T \bar{\mathbf{D}} \mathbf{B}_2 + \mathbf{B}_2^T \bar{\mathbf{F}} \mathbf{B}_3 + \mathbf{B}_3^T \bar{\mathbf{E}} \mathbf{B}_1 \\ &+ \mathbf{B}_3^T \bar{\mathbf{F}} \mathbf{B}_2 + \mathbf{B}_3^T \bar{\mathbf{H}} \mathbf{B}_3 + \mathbf{B}_4^T \hat{\mathbf{A}} \mathbf{B}_4 + \mathbf{B}_4^T \hat{\mathbf{B}} \mathbf{B}_5 + \mathbf{B}_5^T \hat{\mathbf{B}} \mathbf{B}_4 + \mathbf{B}_5^T \hat{\mathbf{D}} \mathbf{B}_5\end{aligned}\quad (25)$$

The bending solutions can be obtained by solving the following equation

$$\mathbf{Kd} = \mathbf{F} \quad (26)$$

On the other hand, the kinetic energy is written as

$$T = \frac{1}{2} \int_{V_e} \dot{\mathbf{u}}_0^T \boldsymbol{\rho}(z) \dot{\mathbf{u}}_0 dV = \frac{1}{2} \dot{\mathbf{q}}_e^T \left\{ \int_{V_e} \mathbf{N}^T \mathbf{L}^T \boldsymbol{\rho}(z) \mathbf{L} \mathbf{N} dV \right\} \dot{\mathbf{q}}_e = \frac{1}{2} \dot{\mathbf{q}}_e^T \mathbf{M}_e \dot{\mathbf{q}}_e \quad (27)$$

$$\mathbf{L} = \begin{bmatrix} 1 & 0 & \left(\frac{1}{4} z - \frac{5}{3h^2} z^3 \right) \frac{\partial}{\partial x} & \frac{5}{4} \left(z - \frac{4}{3h^2} z^3 \right) & 0 \\ 0 & 1 & \left(\frac{1}{4} z - \frac{5}{3h^2} z^3 \right) \frac{\partial}{\partial y} & 0 & \frac{5}{4} \left(z - \frac{4}{3h^2} z^3 \right) \\ 0 & 0 & 1 & 0 & 0 \end{bmatrix} \quad (28)$$

Then, the mass matrix of element is given by

$$\mathbf{M}_e = \int_{V_e} \mathbf{N}^T \mathbf{L}^T \boldsymbol{\rho}(z) \mathbf{L} \mathbf{N} dV = \int_{S_e} \mathbf{N}^T \left(\int_{-h/2}^{h/2} \boldsymbol{\rho}(z) \mathbf{L}^T \mathbf{L} dz \right) \mathbf{N} dS \quad (29)$$

The frequency equation can be solved by

$$(\mathbf{K} - \omega^2 \mathbf{M})\mathbf{d} = 0 \tag{30}$$

3.0 NUMERICAL SOLUTIONS

To verify the application of this procedure, the square structure, $b/a = 1$, $a/h = 10$, with fully simply supported (SSSS) and made of $Si_3N_4/SUS304$, is tested with a uniform load q . Besides, the mesh 20×20 is used in this paper for all examples. The material properties are presented in Table 1. The dimensionless centre deflections $\bar{w} = [100w_c E_m h^3] / [12(1 - \nu_m^2) q a^4]$ can be obtained and compared with the analytical solutions from [12] in Table 2. As expected, the present numerical results reveal good agreements with reference exact solutions.

Now, a functionally graded sandwich plate, $b/a = 1$, with one homogenous ceramic core of ZrO_2 and two functionally graded skins of Al/ZrO_2 is studied. Young's modulus of ZrO_2 and Al are shown in Table 1, while the Poisson's ratio is constant at 0.3, and the ratio a/h equals to 10. The (SSSS) condition is used and the plate is subjected to sinusoidal load q_s . The dimensionless centre deflection is computed as in the following formula $\bar{w} = [10w_c E_o h] / [q_s a^2]$ with $E_o = 1$ GPa. Table 3 shows the comparison of these values under Type I by changing the porosity factor e with the results from paper [13] using an analytical solution. It is obvious that these numerical results approximate to the results of [13], respectively.

Furthermore, the numerical solutions for bending analysis of functionally graded sandwich plates, $b/a = 1$, $a/h = 10$, contain one homogenous ceramic core of Al_2O_3 , one bottom skin of Al/Al_2O_3 and one top skin of $SUS304/Al_2O_3$. The material properties of $SUS304$ are changed by $E_t = 207$ GPa, $\nu = 0.3$. The effective Young's modulus is also demonstrated in Figures 2 and 3. Table 4 shows the dimensionless centre deflections of fully clamped (CCCC) plates under Type II by changing the porosity factor e . It is clearly seen that as e increases, the deflection increases due to the decrease in structural stiffness, except for the case [1/0/1] because there is no longer a middle core.

Table 1: The material properties

SUS304	$E_m = 207.79$ GPa, $\nu = 0.3176$
Si_3N_4	$E_c = 322.27$ GPa, $\nu = 0.24$
ZrO_2	$E_c = 151$ GPa, $\nu = 0.3$
Al	$E_m = 70$ GPa, $\nu = 0.3$
Al_2O_3	$E_c = 380$ GPa, $\nu = 0.3$

Table 2: The comparison of dimensionless center deflections

$n = 0.5$		$n = 1$		$n = 5$		$n = 10$	
[12]	Present	[12]	Present	[12]	Present	[12]	Present
0.325	0.325	0.343	0.346	0.380	0.384	0.396	0.399

Table 3: The comparison of the dimensionless center deflection with porosity related to Type I, $n = 2$, $b/a = 1$, (SSSS) condition and material properties of $Al/ZrO_2 + ZrO_2$

E	Comparison	[1/0/1]	[1/1/1]	[2/2/1]
0	Present	0.3636	0.3193	0.3012
	[13]	0.3732	0.3328	0.3116
0.1	Present	0.4251	0.3603	0.3342
	[13]	0.4415	0.3840	0.3596

Table 4: The dimensionless center deflection with porosity related to Type II, $n = 2$, $b/a = 1$, (CCCC) condition and material properties of $Al/Al_2O_3 + Al_2O_3 + SUS304/Al_2O_3$

e	[1/0/1]	[1/1/1]	[2/2/1]
0	0.0697	0.0556	0.0565
0.1	0.0697	0.0560	0.0570
0.2	0.0697	0.0563	0.0574
0.3	0.0697	0.0567	0.0580

On the other hand, for frequency analysis, a functionally graded sandwich plate, $b/a = 1$, $a/h = 10$, contains one homogenous ceramic core of Al_2O_3 , and two skins of Al/Al_2O_3 are considered. Some further material properties are given as $\rho_{core} = 3800 \text{ kg/m}^3$, $\rho_{bottom} = \rho_{top} = 2707 \text{ kg/m}^3$. The first dimensionless frequencies $\bar{\omega} = \omega \frac{a^2}{h} \sqrt{\frac{\rho_0}{E_0}}$ related to Type I, $n = 2$, (SSSS) condition and based on this procedure, by changing e , are calculated and compared with other solutions from [14]. Note that $\rho_0 = 1$, $E_0 = 1 \text{ GPa}$. Table 5 shows that these numerical results approximate to those of [14]. Besides, the first six mode shapes for this plate with case of ratio of the thicknesses [1/1/1] and $e = 0.1$ are also depicted in Figure 4. The disappearance of spurious modes in vibration analysis can be considered as an advantage of this proposed method. The errors are not large due to different approaches, so they can be ignored in this study.

Table 5: The comparison of the first dimensionless frequency with porosity related to Type I, $n = 2$, $b/a = 1$, $a/h = 10$, (SSSS) condition and material properties of $Al/Al_2O_3 + Al_2O_3$

E	Comparison	[1/0/1]	[1/1/1]	[2/2/1]
0	Present	1.0867	1.2112	1.2548
	[14]	1.0616	1.1885	1.2139
0.1	Present	1.0314	1.1499	1.2252
	[14]	0.9826	1.1207	1.1819
0.2	Present	0.9013	1.0782	1.1625
	[14]	0.8787	1.0420	1.1105

Table 6: The first dimensionless frequency with porosity related to Type II, $n = 2$, $b/a = 1$, $a/h = 10$, (CCCC) condition and material properties of $Al/Al_2O_3 + Al_2O_3 + SUS304/Al_2O_3$

e	[1/0/1]	[1/1/1]	[2/2/1]
0	1.8595	2.1636	2.2579
0.1	1.8595	2.1713	2.2689
0.2	1.8595	2.1790	2.2799
0.3	1.8595	2.1866	2.2910

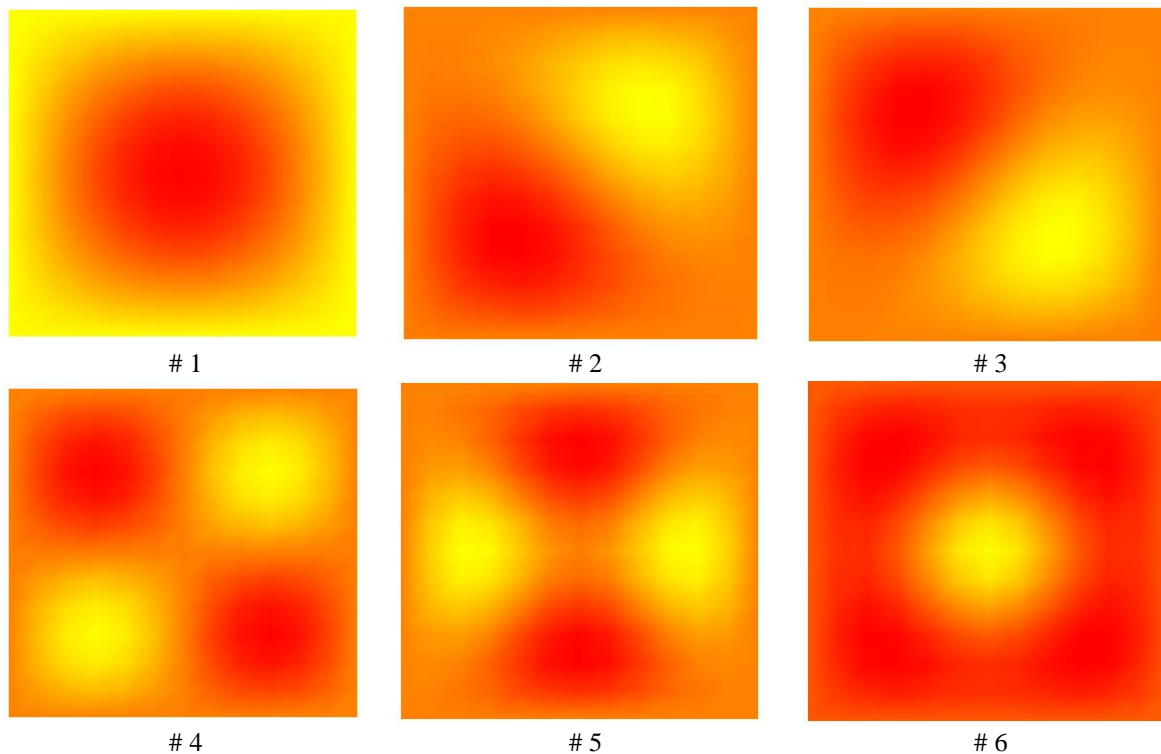


Figure 4. The first six mode shapes for functionally graded sandwich square plate with ratio of the thicknesses [1/1/1], Type I, material properties of $Al/Al_2O_3 + Al_2O_3$, $n = 2$, $e = 0.1$ and (SSSS) condition.

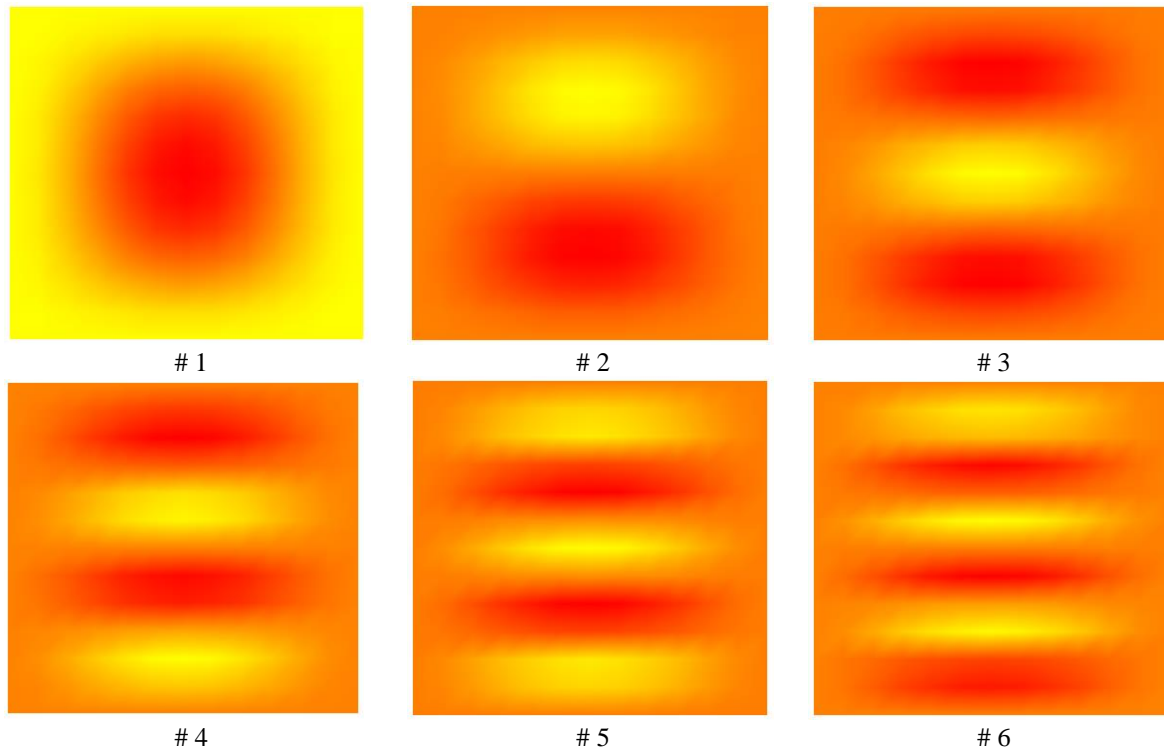


Figure 5. The first six mode shapes for functionally graded sandwich plate with $b/a = 4$, $a/h = 10$, ratio of the thicknesses [2/2/1], Type II, material properties of $Al/Al_2O_3 + Al_2O_3 + SUS304/Al_2O_3$, $n = 2$, $e = 0.1$ and (CCCC) condition.

Finally, the first dimensionless frequencies by changing porosity factor e for a functionally graded sandwich plate related to Type II, $n = 2$, $b/a = 1$, $a/h = 10$, (CCCC) condition and material properties of $Al/Al_2O_3 + Al_2O_3 + SUS304/Al_2O_3$ are presented in Table 6. Note that $\rho_{core} = 3800 \text{ kg/m}^3$, $\rho_{bottom} = 2707 \text{ kg/m}^3$ and $\rho_{top} = 8166 \text{ kg/m}^3$ for this analysis. Figure 5 demonstrates the first six mode shapes of this plate by replacing b/a from 1 to 4 and e equals 0.1 for another view.

4.0 CONCLUSION

Using the recommended element in the numerical investigation has several benefits within the context of the C^0 -HSDT model. This study has successfully applied the analysis of PFGS plates and provided results without needing shear-correct factors. It is additionally pointed out that this C^0 -HSDT related element does not require a large computing cost as it just makes use of bilinear function approximations. Besides, after performing numerical instances, it is discovered that this element does not exhibit shear locking or the hourglass phenomenon; thus, it produces results that are satisfactory when compared to other published solutions from earlier studies. The computational approximation of this procedure and the influences of various parameters like porosity factor, volume fraction index, or geometric ratio on the bending and vibration of PFGS plates are also studied. Moreover, this paper helps to supplement the knowledge of engineers in reality. Last but not least, in the near future, this element type can be further extended to the geometrically nonlinear analysis of plate or shell structures.

ACKNOWLEDGEMENT

The author received no financial support for the research, authorship, or publication.

REFERENCES

- [1] J. Kim and J. N. Reddy, "Analytical solutions for bending, vibration, and buckling of FGM plates using a couple stress-based third-order theory," *Compos Struct*, vol. 103, pp. 86-98, 2013.
- [2] K. Swaminathan and D. T. Naveenkumar, "Higher order refined computational models for the stability analysis of FGM plates – Analytical solutions," *Eur J Mech A-Solid*, vol. 47, pp. 349-361, 2014.
- [3] S. J. Singh and S. P. Harsha, "Thermo-mechanical analysis of porous sandwich S-FGM plate for different boundary conditions using Galerkin Vlasov's method: A semi-analytical approach," *Thin Wall Struct*, vol. 150, p. 106668, 2020.

- [4] N. Magouh, L. Azrar and K. Alnefae, "Semi-analytical solutions of static and dynamic degenerate, nondegenerate and functionally graded electro-elastic multilayered plates," *Appl Math Model*, vol. 111, pp. 722-744, 2023.
- [5] G. Shi, "A new simple third-order shear deformation theory of plates," *Int J Solids Struct*, vol. 44, pp. 4399-4417, 2007.
- [6] A. M. Katili and I. Katili, "Improving Felippa Bergan Triangular element by using UI approach for analysis of isotropic and FGM sandwich plates," *Compos Struct*, vol. 312, p. 116823, 2023.
- [7] S. Pandey and S. Pradyumna, "Analysis of functionally graded sandwich plates using a higher-order layerwise theory," *Compos Part B-Eng*, vol. 153, pp. 325-336, 2018.
- [8] M. D. Sciuva and M. Sorrenti, "Bending, free vibration and buckling of functionally graded carbon nanotube-reinforced sandwich plates, using the extended Refined Zigzag Theory," *Compos Struct*, vol. 227, p. 111324, 2019.
- [9] M. Dorduncu, "Stress analysis of sandwich plates with functionally graded cores using peridynamic differential operator and refined zigzag theory," *Thin Wall Struct*, vol. 146, p. 106468, 2020.
- [10] J. L. Mantari and E. V. Granados, "A refined FSDT for the static analysis of functionally graded sandwich plates," *Thin Wall Struct*, vol. 90, pp. 150-158, 2015.
- [11] H. L. Ton-That, "Finite element analysis of functionally graded skew plates in thermal environment based on the new third-order shear deformation theory," *J Appl Comput Mech*, vol. 6, pp. 1044-1057, 2020.
- [12] N. Wattanasakulpong, G. B. Prusty and D. W. Kelly, "Free and forced vibration analysis using improved third-order shear deformation theory for functionally graded plates under high temperature loading," *J Sandw Struct Mater*, vol. 15, pp. 583-606, 2013.
- [13] A. M. Zenkour, "A comprehensive analysis of functionally graded sandwich plates: Part 1 Deflection and stresses," *Int J Solids Struct*, vol. 42, pp. 5224-5242, 2005.
- [14] A. M. Zenkour, "A comprehensive analysis of functionally graded sandwich plates: Part 2 buckling and free vibration," *Int J Solids Struct*, vol. 42, pp. 5243-5258, 2005.
- [15] B. L. Liu, S. Li and Y. S. Li, "Bending of FGM sandwich plates with tunable auxetic core using DQM," *Eur J Mech A-Solid*, vol. 97, p. 104838, 2023.
- [16] S. S. Tomar and M. Talha, "Influence of material uncertainties on vibration and bending behaviour of skewed sandwich FGM plates," *Compos Part B-Eng*, vol. 163, pp. 779-793, 2019.
- [17] M. M. Alipour and M. Shariyat, "Analytical stress analysis of annular FGM sandwich plates with non-uniform shear and normal tractions, employing a zigzag-elasticity plate theory," *Aerosp Sci Technol*, vol. 32(1), pp. 235-259, 2014.
- [18] N. N. Beni and M. B. Dehkordi, "An extension of Carrera unified formulation in polar coordinate for analysis of circular sandwich plate with FGM core using GDQ method," *Compos Struct*, vol. 185, pp. 421-434, 2018.
- [19] F. Moleiro, V. M. F. Correia, A. J. M. Ferreira and J. N. Reddy, "Fully coupled thermo-mechanical analysis of multilayered plates with embedded FGM skins or core layers using a layerwise mixed model," *Compos Struct*, vol. 210, pp. 971-996, 2019.
- [20] D. Li, Z. Deng, H. Xiao and P. Jin, "Bending analysis of sandwich plates with different face sheet materials and functionally graded soft core," *Thin Wall Struct*, vol. 122, pp. 8-16, 2018.
- [21] A. Alibeigloo and M. Alizadeh, "Static and free vibration analyses of functionally graded sandwich plates using state space differential quadrature method," *Eur J Mech A-Solid*, vol. 54, pp. 252-266, 2015.
- [22] D. P. Bhaskar, S. V. Bhaskar, S. S. Raj and L. S. Dhamande, "Numerical investigation of sandwich plate in bending by a new inverse shear deformation theory based on finite element analysis," *Forces Mech.*, vol. 13, p. 100238, 2023.
- [23] L. H. T. That, "Four-node quadrilateral C^0 -element based on cell-based smoothed strains strategy and third-order shear deformation theory for functionally graded carbon nanotube reinforced composite plates," *Raken. Mek.*, vol. 56(1), p. 1-23, 2023.
- [24] H. L. Ton-That, "Plate structural analysis based on a double interpolation element with arbitrary meshing," *Acta Mech. et Autom.*, vol. 15(2), pp. 91-99, 2021.
- [25] H. L. Ton-That, "A new C^0 third-order shear deformation theory for the nonlinear free vibration analysis of stiffened functionally graded plates," *Facta Univ. Ser.: Mech. Eng.*, vol. 19(2), pp. 285-305, 2021.
- [26] H. L. Ton-That, "A novel quadrilateral element for dynamic response of plate structures subjected to blast loading," *J Appl Comput Mech*, vol. 6, pp. 1314-1323, 2020.
- [27] H. Dang-Trung, D. J. Yang and Y. C. Liu, "Improvements in shear locking and spurious zero energy modes using Chebyshev finite element method," *J. Comput. Inf. Sci. Eng.*, vol. 19(1), p. 011006, 2019.
- [28] T. Chau-Dinh, T. K. Nguyen, H. Nguyen-Van and H. L. Ton-That, "A MITC3+ element improved by edge-based smoothed strains for analyses of laminated composite plates using the higher-order shear deformation theory," *Acta Mech*, vol. 232, pp. 389-422, 2021.

- [29] T. Q. Bui, T. V. Do, L. H. T. Ton, D. H. Doan, S. Tanaka, D. T. Pham, T. A. Nguyen-Van, T. Yu and S. Hirose, "On the high temperature mechanical behaviors analysis of heated functionally graded plates using FEM and a new third-order shear deformation plate theory," *Compos Part B-Eng*, vol. 92, pp. 218-241, 2016.
- [30] H. L. Ton-That, H. Nguyen-Van and T. Chau-Dinh, "A novel quadrilateral element for analysis of functionally graded porous plates/shells reinforced by graphene platelets," *Arch. Appl. Mech.*, vol. 91, pp. 2435-2466, 2021.